


Relation between disorder and homogeneity in an amorphous metalZ. Ovadyahu *Racah Institute of Physics, The Hebrew University, Jerusalem 9190401, Israel*

(Received 21 August 2022; revised 20 October 2022; accepted 31 October 2022; published 10 November 2022)

Disorder and homogeneity are two concepts that refer to spatial variation of the system potential. In condensed-matter systems disorder is typically divided into two types: with local parameters varying from site to site (diagonal disorder) and those characterized by random transfer-integral values (off-diagonal disorder). Amorphous systems in particular exhibit off-diagonal disorder due to random positions of their constituents. In real systems diagonal and off-diagonal disorder may be interconnected. The formal depiction of disorder as local deviations from a common value focuses attention on the short-range components of the potential landscape. However, long-range potential fluctuations are quite common in real systems. In this paper we seek to find a correlation between disorder and homogeneity using amorphous indium-oxide (In_xO) films with different carrier concentrations and with different degree of disorder. Thermal treatment is used as a means of fine tuning the system disorder. In this process the resistance of the sample decreases while its amorphous structure and chemical composition is preserved. The reduced resistivity affects the Ioffe-Regel parameter $k_F\ell$ that is taken as a relative measure of disorder in a given sample. The homogeneity of the system was monitored using inelastic light-scattering. This is based on collecting the Raman signal from micron-size spots across the sample. The statistics of these low-energy data are compared with the sample disorder independently estimated from transport measurements. The analysis establishes that heterogeneity and disorder are correlated.

DOI: [10.1103/PhysRevB.106.184205](https://doi.org/10.1103/PhysRevB.106.184205)**I. INTRODUCTION**

Disorder plays a major role in the properties of condensed-matter systems [1–9]. The experimental study of disorder-induced phenomena present a challenge in terms of being able to control, characterize, and quantify it. Effort in this vein was mainly invested in the field of electronic transport. In particular, this issue has been a major concern in studies of the metal-insulator transition (MIT) and the superconductor-insulator transition (SIT). The system conductivity is frequently used as an empirical measure of disorder in these studies. The conductivity of a solid is arguably its most sensitive property and it may be affected by different means, not all of them may be attributed to disorder. A change in carrier concentration, for example, would affect the conductivity while causing only a small change in the disorder.

An aspect of disorder frequently referred to, but rarely actually measured, is homogeneity. It should be realized that the two concepts are related; spatial disorder is tantamount to inhomogeneous. Strong disorder, such as required to Anderson-localize a system with a relatively high carrier concentration, is naturally accompanied by significant spatial variations of the potential. We shall refer to this type of inhomogeneity as “inherent”. A system may, however, be inhomogeneous with little or no short-range potential fluctuations being present. This form of “technological” inhomogeneity [10,11] may lead to nontrivial transport effects in otherwise “clean” systems. In principle, the two types of inhomogeneities may be told apart; changing the disorder should show a concomitant change of inhomogeneity if the disorder is inherent.

As a relevant example, we present in this note experiments to study the relation between disorder and spatial inhomogeneity in amorphous indium-oxide (In_xO) films. Using a purely amorphous system for this project is natural; the only structurally imposed length-scale is the nearest-neighbor distance, which turns out to be much smaller than any dimension relevant to the problem. This research focused on the version of the material that is relatively rich in carrier concentration. This version of In_xO has been extensively studied and its transport parameters are well known [12,13]. In particular, near the critical point of the MIT the magnitude of the disorder may be quantitatively determined from the condition for the Anderson transition. The heterogeneity at this disorder is compared with another version of In_xO that topologically is nearly identical while much less disordered. Subjecting both systems to thermal treatment that modifies their resistivities allows for another way to test the effect of disorder on system homogeneity. The sample disorder before and after heat treatment is characterized by the Ioffe-Regel parameter $k_F\ell$. Low-energy Raman spectroscopy is employed to probe the system spatial homogeneity in each case for tracking the change associated with the modified disorder. The results support the expected notion that heterogeneity is an inherent property of the disordered system.

II. EXPERIMENTAL**A. Samples preparation and measurements techniques**

The In_xO films used in this paper were e-gun evaporated onto room-temperature substrates using 99.999% pure In_2O_3

sputtering target. Deposition was carried out at the ambience pressure of $3 \pm 0.5 \times 10^{-5}$ to $4 \pm 0.5 \times 10^{-4}$ Torr oxygen pressure maintained by leaking 99.9% pure O_2 through a needle valve into the vacuum chamber (base pressure $\approx 10^{-6}$ Torr). Undoped silicon wafers with $\langle 100 \rangle$ orientation were used as substrates for electrical and Raman measurements. Carbon-coated copper grids were used for transmission electron-diffraction. During film deposition, the grids were anchored to 1-mm glass slides by small indium pellets later removed for mounting the grids in the microscope. The deposited film on the rest of the slide was used for monitoring the sample resistance for comparison. x-ray interferometry was performed on samples deposited on a 2.8-mm float-glass.

Rates of deposition in the range 0.3–2.5 Å/s were used to produce films with different compositions. The In_xO samples had carrier concentration N that increases with the ratio of deposition rate to the oxygen partial pressure. For the rates pressures used here N was in the range $1 \times 10^{19} \text{ cm}^{-3}$ to $9 \times 10^{20} \text{ cm}^{-3}$ as measured by Hall effect at room temperature using a Hall-bar control sample prepared simultaneously for each sample deposition. Lateral sizes of samples used for transport measurements was typically $1 \times 2.5 \text{ mm}^2$ (width \times length respectively), and $1 \times 1 \text{ cm}^2$ for the Raman scattering experiments. The evaporation source to substrate distance in the deposition chamber was $45 \pm 1 \text{ cm}$. Therefore, thickness variations across the samples are unlikely to be related to geometrical consideration in the deposition process.

To afford reasonable resolution for electron microscopy thickness of the films used for the electron-microscope work was $d = 20 \pm 1 \text{ nm}$.

Two batches of In_xO with carrier concentrations of $N = (1.5 \pm 1) \times 10^{19} \text{ cm}^{-3}$, and $N = (8 \pm 1) \times 10^{20} \text{ cm}^{-3}$ were deposited for the Raman scattering experiments. In the following these will be referred to as “low- N ” and “high- N ” versions of In_xO respectively. The high- N version may be also referred to in this paper as the “indium-rich” phase of the compound. These version of In_xO are representative for the substance used in recent electron-glass experiments with typically $N \approx 10^{19} \text{ cm}^{-3}$ and the In_xO version with $N \approx 10^{21} \text{ cm}^{-3}$ commonly used in superconductor-insulator studies [14–22].

The Ioffe-Regel parameter $k_F \ell = (9\pi^4/N)^{1/3} \frac{R_Q}{\rho_{RT}}$ where $R_Q = \hbar/e^2$ is the resistance quantum and ρ_{RT} is the resistivity at room temperature, is used here as a measure of the sample relative disorder. This parameter is monotonic with disorder, and it is well defined experimentally. It is descriptive of the static disorder even when its value is smaller than unity where neither k_F nor ℓ are “good” parameters (which is the case in all our “as-made” samples). The important caveat that should be borne in mind in this regard is that when $k_F \ell \ll 1$, ℓ must not be interpreted as a semiclassical mean-free-path. At room temperatures, where our measurements are performed, it is safe to say that the transport length-scale (whether it is the hopping-length or the mean-free-path) is *much* smaller than the size of the region probed by the laser beam.

Sample homogeneity on a micron-scale was characterized by the intensity variations of the Raman signal over the energy range 70–420 cm^{-1} . These were carried for In_xO samples with different N as well as for the as-made and the annealed samples where disorder was modified by thermal treatment.

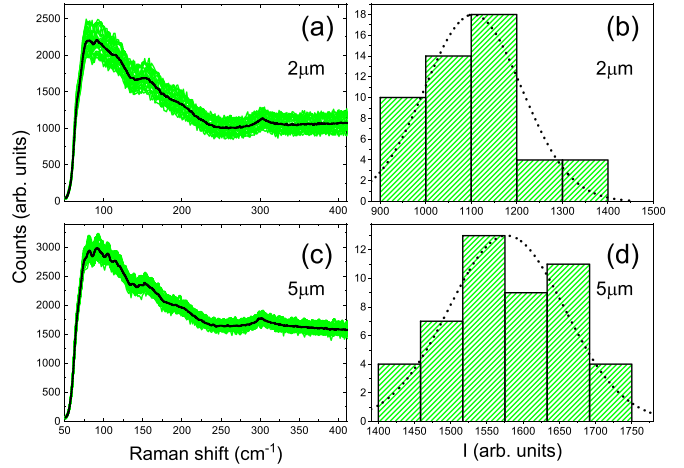


FIG. 1. Raman spectra for the as-made In_xO sample with $N \approx 8 \times 10^{20} \text{ cm}^{-3}$. The sheet resistance of the film $R_{\square} = 18.34 \text{ k}\Omega$, at room temperature, which yields $k_F \ell = 0.1$. [(a), (c)] The Raman shift vs energy for fifty different local sampling points using $2 \mu\text{m}$ and $5 \mu\text{m}$ spot size respectively. The black line is the average of the 50 plots. [(b), (d)] The histogram of the Raman intensity-plots averaged over the interval 350–400 cm^{-1} for each of the local readings related to the $2 \mu\text{m}$ and $5 \mu\text{m}$ spot size respectively. The histograms in (b) and (d) are fitted to normal distributions depicted as dashed lines. These fits yield heterogenous parameters (see text for definition) $\gamma = 9.7\%$ for the $2 \mu\text{m}$ spot size and $\gamma = 5.1\%$ for the $5 \mu\text{m}$ spot size.

Electron diffraction patterns were taken with the Philips Tecnai F20 G2 operating at 200 kV. The Raman spectra were taken with a Renishaw inVia Reflex Spectrometer using a laser beam with a wavelength of 514 nm and edge filter at $\approx 70 \text{ cm}^{-1}$. These measurements employed beam spots of $2 \mu\text{m}$ and $5 \mu\text{m}$. In each case, fifty spectra were taken at different spots across a rectangle area of the sample for obtaining statistics of the Raman signal magnitude. The laser intensity was checked to be in the linear response and low enough to avoid structural changes during exposure [23]. During these preliminary tests, the *same* spot on the sample was measured several times. Traces were taken from this spot with different laser intensities. The spot could be identified in the microscope as it changed color after several exposures. However, the Raman traces taken from it registered the same spectrum over the range studied with intensity variations of typically $\pm 0.5\%$. Therefore the variations of signal intensity reported below are mostly due to inhomogeneities rather than due to time dependence.

The deposited samples, after being characterized, were heat treated to modify their disorder at $T = 360 \pm 5 \text{ K}$ for 24–48 hours. Fuller details related to heat treatment of In_xO films are described elsewhere [24].

III. RESULTS AND DISCUSSION

Local Raman spectra for the high- N version In_xO film are shown in Fig. 1 for the as-made, indium-rich sample. As mentioned above, this version of In_xO has been often used for the disorder-driven SIT. This transition occurs when the Ioffe-Regel parameter $k_F \ell$ of the system is 0.29–0.32 [25]. Figure 2 shows the respective set of data for the same sample after it

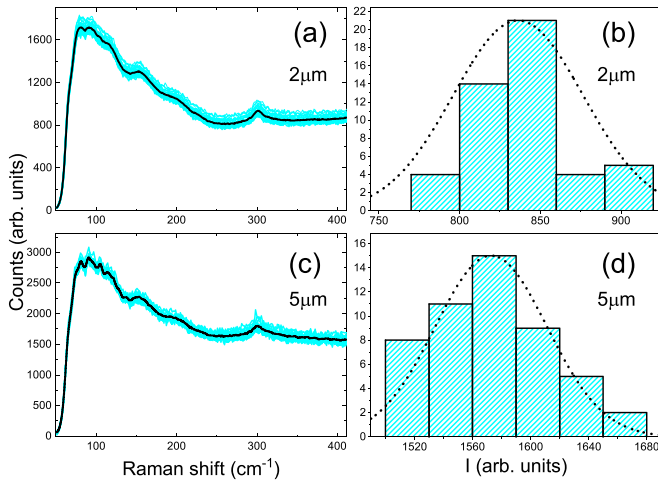


FIG. 2. Raman spectra for the In_xO sample with $N \approx 8 \times 10^{20} \text{cm}^{-3}$ after being heat treated at $\approx 380 \text{ K}$ for ≈ 48 hours. The sheet resistance of the film changed to $R_{\square} = 3.95 \text{ k}\Omega$, which gives $k_{\text{F}}\ell = 0.42$. [(a), (c)] The Raman shift vs energy for fifty different local sampling points using $2 \mu\text{m}$ and $5 \mu\text{m}$ spot size respectively. The black line is the average of the 50 plots. [(b), (d)] The histogram of the Raman intensity plots averaged over the interval $350\text{--}400 \text{ cm}^{-1}$ for each of the local readings related to the $2 \mu\text{m}$ and $5 \mu\text{m}$ spot size respectively. The histograms in (b) and (d) are fitted to normal distributions depicted as dashed lines. These fits yield heterogenous parameters (see text for definition) $\gamma = 4.9\%$ (down from $\gamma = 9.7\%$ in the as-made sample) for the $2 \mu\text{m}$ spot size and $\gamma = 2.5\%$ (down from $\gamma = 5.1\%$ in the as-made sample) for the $5 \mu\text{m}$ spot size.

has been heat treated and its $k_{\text{F}}\ell$ value has increased from 0.1 to 0.42. The data in Figs. 1 and 2 pertain therefore to the insulating and superconducting side of the SIT respectively.

Two features stand out in these data: First, the local intensity of the Raman signal fluctuates considerably from point to point [Figs. 1(a) and 1(c)] manifesting the spatial heterogeneity of the sample. Second, homogeneity of the sample visibly improves after heat treatment [Figs. 2(a) and 2(c)]. The sample heterogeneity parameter γ is defined here as a ratio $\gamma \equiv [\text{standard deviation}]/[\text{mean}]$ of a normal distribution fitted to the intensity histogram. The use of normal distribution to fit the histogram data is just to allow an impartial estimate of the sample heterogeneity. To determine the precise functional form of the distribution would require many more data plots than used here. Nonetheless, the obtained data are consistent and systematic enough to test the basic conjecture concerning the disorder-homogeneity relation. Note that γ is smaller for the annealed sample, and it is smaller for the larger spot size as might be expected from the better ensemble averaging.

Before proceeding, the natural question is what is reflected by the magnitude of the Raman signal?

At the energy range studied $\varepsilon = 70\text{--}420 \text{ cm}^{-1}$, the signal is composed of two components associated with different inelastic light-scattering mechanisms. For energies $\varepsilon \leq 250 \text{ cm}^{-1}$, the main contribution comes from the boson peak [26–32] of the amorphous material. This feature, related to the phonon system of In_xO , has been studied previously as function of disorder and composition [23]. The other component is presumably inelastic scattering from the electronic

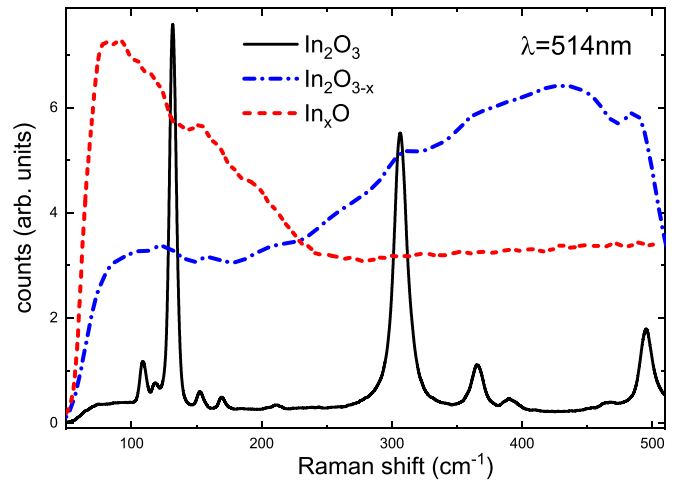


FIG. 3. Raman spectra characteristic of three different versions of indium-oxide films. The plot labeled as In_2O_3 (full line) is based on data taken from the source material used in this paper for depositing the films. The In_xO (dashed line) is taken from a 90-nm-thick amorphous film. The polycrystalline version of indium oxide (dotted-dashed line) was crystallized and further heat treated at $\approx 700 \text{ K}$ for 25 min. to form $\text{In}_2\text{O}_{3-x}$. The extended heat treatment at elevated temperature was needed to remove any residue of amorphous component. The latter would otherwise show up as an excess signal at the boson peak energy. Note that the boson peak does not appear in either of the polycrystalline versions.

states, either extended or weakly localized in the presence of quenched disorder.

To illustrate the relevance of this electronic mechanism for this material, consider the Raman data shown in Fig. 3. Note the different spectra for the two polycrystalline versions of indium oxide. These samples share the same crystal structure with a body-centered cubic symmetry [33]. The grain size of the In_2O_3 may be somewhat larger than in the deposited film $\text{In}_2\text{O}_{3-x}$ but this cannot explain the grossly different Raman spectra. A likely relevant difference between the compounds is their chemical stoichiometry; the vacuum-deposited film $\text{In}_2\text{O}_{3-x}$ is 8–10% oxygen deficient [33] that, in turn, renders the system metallic with carrier-concentration $N \approx 5 \times 10^{19} \text{ cm}^{-3}$. The In_2O_3 sample on the other hand is actually an intrinsic semiconductor with $N \approx 10^{16} \text{ cm}^{-3}$ as measured by Hall effect at room temperature. It is then plausible to associate the distinctive spectrum of the $\text{In}_2\text{O}_{3-x}$ with an electronic mechanism for inelastic light scattering [34], similar to the findings in underdoped cuprate [35].

Evidently, the electronic contribution to the Raman signal is substantial. It overwhelms the Raman-active material vibration modes and those that appear are shifted in energy from the positions of their stoichiometric compound.

Note that the prominent boson peak portrayed by the amorphous sample is absent (or is very weak) in either crystalline specimen. This is a demonstration of the difference sensitivity of phonons and electrons to different types of disorder; the grain size in both, $\text{In}_2\text{O}_{3-x}$ films and In_2O_3 sputtering-target pieces is at least $0.5 \mu\text{m}$, much larger than the mean-free-path for electrons in samples where $k_{\text{F}}\ell < 1$. The large wavelength of phonons makes them less sensitive to the short-range

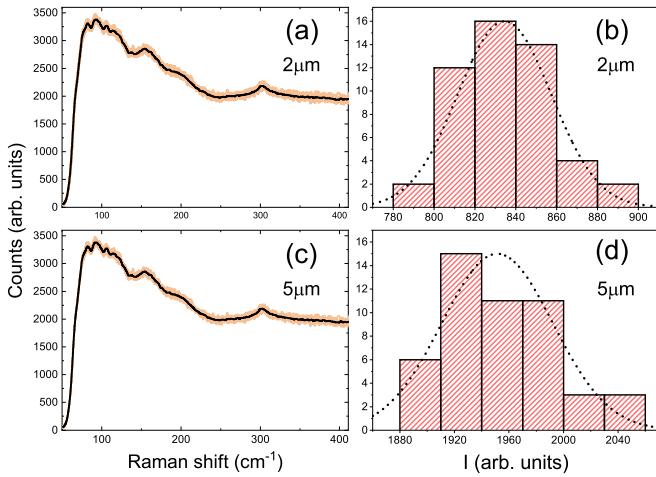


FIG. 4. Raman spectra for the as-made In_xO sample with $N \approx 1 \times 10^{19} \text{ cm}^{-3}$. The original sheet resistance of the film $R_{\square} = 1.3 \text{ M}\Omega$, at room temperature, which yields $k_{\text{F}}\ell = 0.005$. [(a), (c)] The Raman shift vs energy for fifty different local sampling points using $2 \mu\text{m}$ and $5 \mu\text{m}$ spot size respectively. The black line is the average of the 50 plots. [(b), (d)] The histogram of the Raman intensity plots averaged over the interval $350\text{--}400 \text{ cm}^{-1}$ for each of the local readings related to the $2 \mu\text{m}$ and $5 \mu\text{m}$ spot size respectively. The histograms in (b) and (d) are fitted to normal distributions depicted as dashed lines. These fits yield heterogenous parameters (see text for definition) $\gamma = 2.7\%$ for the $2 \mu\text{m}$ spot size and $\gamma = 2.1\%$ for the $5 \mu\text{m}$ spot size.

fluctuations of the chemical composition which strongly affects charge carriers. Hence the effective Ioffe-Regel parameter for phonons $(k_{\text{F}}\ell)_{\text{ph}}$ may be larger than unity, thus unfavorable to exhibit a boson peak in the phonon density-of-states [28].

In contrast with good metals, Raman signal from “free” electrons is possible in strongly disordered metals. The underlying physics has been considered in [34]. The theory strictly applies to $k_{\text{F}}\ell > 1$ regime yet light-induced fluctuations of the chemical potential and the ensuing relaxation of electron-hole pairs should still survive in strongly-localized In_xO films. The intensity of low-frequency radiation depends mainly on the charge concentration as demonstrated in high- T_{C} compounds [35]. This means that the fluctuation of the Raman intensity depicted in Figs. 1 and 2 essentially signify the variations of carrier concentrations across these region of the sample. This facet of the material affects directly and indirectly the disorder perceived by charge-carriers. The width of the distribution, quantified by the value of γ , is therefore a meaningful measure of the sample heterogeneity averaged over a given length scale.

It is remarkable that significant fluctuations of carrier-concentration are observable over a scale of microns in the high- N sample; γ for the $2 \mu\text{m}$ area is $\approx 10\%$ in the as-made sample and is still $\approx 5\%$ after being annealed [Fig. 2(b)]. Moreover, it is evident from the distribution [Figs. 1(b) and 2(b)] that the probability to find micron-size areas with carrier concentrations that differ by 20–30% is appreciable. This aspect has consequences for the low-temperature transport in such systems in particular, when the observed property is

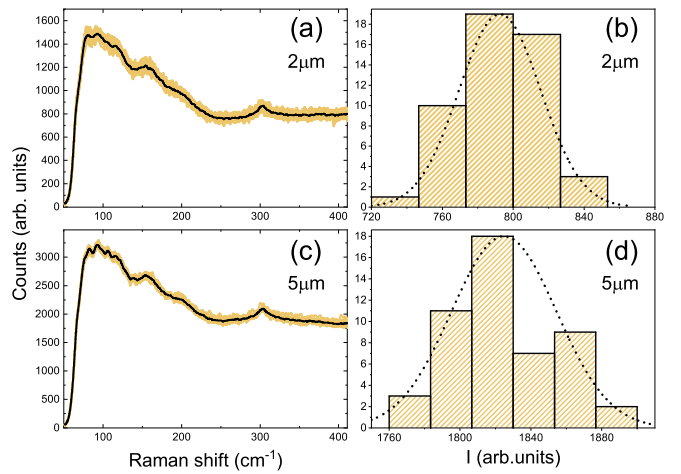


FIG. 5. Raman spectra for the In_xO sample with $N \approx 10^{19} \text{ cm}^{-3}$ after being heat-treated at $\approx 380 \text{ K}$ for ≈ 48 hours. The sheet resistance of the film changed to $R_{\square} = 23 \text{ k}\Omega$, which gives $k_{\text{F}}\ell = 0.29$. [(a), (c)] The Raman shift vs energy for fifty different local sampling points using $2 \mu\text{m}$ and $5 \mu\text{m}$ spot size respectively. The black line is the average of the 50 plots. [(b), (d)] The histogram of the Raman intensity plots averaged over the interval $350\text{--}400 \text{ cm}^{-1}$ for each of the local readings related to the $2 \mu\text{m}$ and $5 \mu\text{m}$ spot size respectively. The histograms in (b) and (d) are fitted to normal distributions depicted as dashed lines. These fits yield heterogenous parameters (see text for definition) $\gamma = 2.8\%$ (compared with $\gamma = 2.7\%$ in the as-made sample) for the $2 \mu\text{m}$ spot size and $\gamma = 1.6\%$ (down from $\gamma = 2.1\%$ in the as-made sample) for the $5 \mu\text{m}$ spot size.

sensitive to the carrier concentration (for example, superconductivity). Indeed, high- N versions of In_xO exhibit anomalous transport effects near their SIT that are ascribed to superconducting islands embedded in an insulating matrix [25] reflecting areas where N is larger than the average value of the sample. Similar emergence of disorder induced “granularity” was found in other metal oxides like high- T_{C} compounds [36–41].

It is illuminating to compare the before-and-after change in γ for this $N \approx 8 \times 10^{20} \text{ cm}^{-3}$ version of the material (Figs. 1 and 2) with the respective behavior in the low- N version sample shown in Fig. 4 and Fig. 5 respectively.

Just by eyeing the raw data (compare Fig. 2 and Fig. 4) it is clear that even the as-made low- N version of In_xO is more homogenous than the heat-treated specimen of the indium-rich material. It is gratifying to see that the respective values of γ are consistent with this observation. This is in line with the notion that heterogeneity is an inherent aspect of disorder in these In_xO films. Table I summarizes the values of γ for the respective samples and states.

Note that the change in γ relative to the change in $k_{\text{F}}\ell$ is considerably weaker in the low- N version.

To understand the reason for these observations and, in particular, the steeper $\partial\gamma/\Delta(k_{\text{F}}\ell)$ in the indium-rich version, we need to expound on the connection between disorder and $k_{\text{F}}\ell$.

In the context of transport, one usually weighs disorder on an energy scale while $k_{\text{F}}\ell$ is dimensionless. A quantitative estimate of disorder is therefore limited to special values of $k_{\text{F}}\ell$ such as its value at the Anderson MIT where the disorder

TABLE I. The inhomogeneous parameter γ (defined in the text), and the change of the sample Ioffe-Regel parameter $\Delta(k_F\ell)$ by heat treatment for the two studied samples. The carrier concentration for the high- N and low- N samples are $N = (8 \pm 1) \times 10^{20} \text{ cm}^{-3}$ and $N = (1.5 \pm 1) \times 10^{19} \text{ cm}^{-3}$ respectively.

	As-made γ (%)		Heat treated γ (%)		$\Delta(k_F\ell)$
	2 μm	5 μm	2 μm	5 μm	
High- N	9.7 ± 0.5	5.1 ± 0.5	4.9 ± 0.5	2.5 ± 0.5	0.32
Low- N	2.7 ± 0.4	2.1 ± 0.4	2.8 ± 0.4	1.6 ± 0.4	0.29

energy may be assessed with respect to E_F [42]. This means that, without specific information on auxiliary properties of a given system, $k_F\ell$ is merely a relative measure of disorder.

Moreover, $k_F\ell$ may be relied on to be indicative of quenched disorder when ρ_{RT} is strictly determined by elastic scattering, a condition that may be obeyed for $k_F\ell$ values at the vicinity of the MIT. The critical $k_F\ell$ in In_xO occurs at $k_F\ell = 0.31 \pm 0.2$ essentially independent of the carrier concentration [25] presumably because the disorder in these samples is always larger than the interaction [43,44]. On the other hand, versions of this material with different N have different degrees of disorder for the same value of $k_F\ell$. In particular, the disorder that brings the system near the Anderson transition, is greater the larger N is. Recall that the critical disorder is associated with potential fluctuations that are large enough to overcome the Fermi energy E_F [42] that in turn increases with the carrier concentration of the system.

For the same reason, for higher N , a larger degree of disorder is required to achieve a given change in $k_F\ell$. This may be illustrated by observing the change in the material optical properties accompanying a reduction of resistivity following heat treatment. Figure 6 shows how the optical gap E_g changes after several heat treatments [45] that progressively increase $k_F\ell$ by reducing ρ_{RT} . E_g signifies the energy scale for transitions between the valence and the conduction bands of In_xO . The figure compares the E_g vs $k_F\ell$ dependence for two ver-

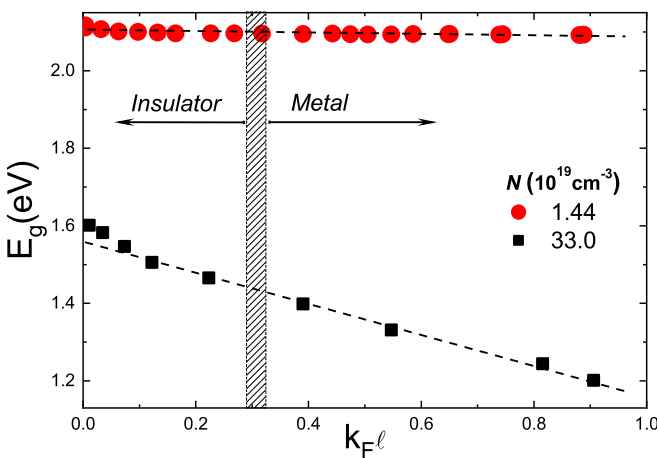


FIG. 6. The dependence of the optical gap E_g on the Ioffe-Regel $k_F\ell$ parameter for two batches of In_xO samples labeled by their respective N . Dashed lines are guides to the eye. Note the much steeper dependence of E_g vs a change in $k_F\ell$ for the sample with the larger N .

sions of In_xO with different carrier concentrations. A change of E_g is a consequence of the system densification [24]. Rearrangement of oxygen vacancies take place concomitantly. Both processes reduce the system disorder. Figure 6 shows that a larger degree of structural change, reflected by ΔE_g , is required to induce a similar change in $k_F\ell$ for the high- N version of In_xO . This is an example of a relation between the energy change required to affect $\Delta(k_F\ell)$ in a specific system.

The two versions of the material differ by their chemical composition, explicitly, by their O/In ratio. For the low- N version in Fig. 6 the ratio is ≈ 1.4 as compared with 1.5 for the stable compound In_2O_3 while it is ≈ 1.25 for the indium-rich version [25]. This relatively small difference in composition leads to a substantial difference in carrier-concentration; the high- N has a larger carrier concentration than the low- N sample in Fig. 6 by a factor of ≈ 23 . This means that their Fermi energies differ by a factor of ≈ 9 , which accounts for the difference in the slopes for $\Delta E_g/\Delta(k_F\ell)$ of the samples. The higher sensitivity of the conductance of the low- N system to changes in the ions potential was offered [46] as the physical reason for the observation that the magnitude of the $1/f$ -noise often scales with the inverse of the carrier concentration (the ‘‘Hooe law’’ [47]).

The fact that, for a similar $k_F\ell$, the high- N sample is more disordered than the low- N sample is not evident from the diffraction patterns of the samples. From the point of view of topology, these two versions are difficult to tell apart; the diffraction patterns comparing between low- N and high- N versions of In_xO films shown in Fig. 7 reveal amorphous structures with nearly identical nearest-neighbor distance for both versions (judging by the strong diffraction-ring diameter).

The additional source of disorder that accounts for the difference between the two versions in Fig. 7 is their deviation from the chemical stoichiometry of the compound. This property is carried by the relatively few valence electrons while diffraction patterns are dominated by scattering from the plentiful inner-shell electrons. Charge carriers that are involved in transport, on the other hand, are equally sensitive to both types of disorder.

To understand the origin of the disorder associated with the lack of stoichiometry, recall that the value of N is determined by the O/In ratio. Oxygen deficiency in indium-oxide specimens is of the order of 10–20% while the observed N is typically smaller by 2–3 orders of magnitude. Therefore some indium atoms must have a valency of +1 rather than the more common +3 to account for the observed N and preserve chemical neutrality [33]. The relative number of these ions determines the carrier concentration while the way they are arranged in space affects the disorder perceived by charge carriers.

The scattering centers for the conduction electrons are actually oxygen vacancies (and possibly, divacancies). Being the lighter element in the compound, oxygen atoms are also the dominant species to diffuse through the sample during heat treatment. Measurement of carrier concentration showed it to be essentially constant during treatment and therefore oxygen movement is essentially confined to within the boundaries of the sample. The constancy of the global carrier concentration was confirmed by three independent means; Hall effect [12], optical absorption [42], and by monitoring the

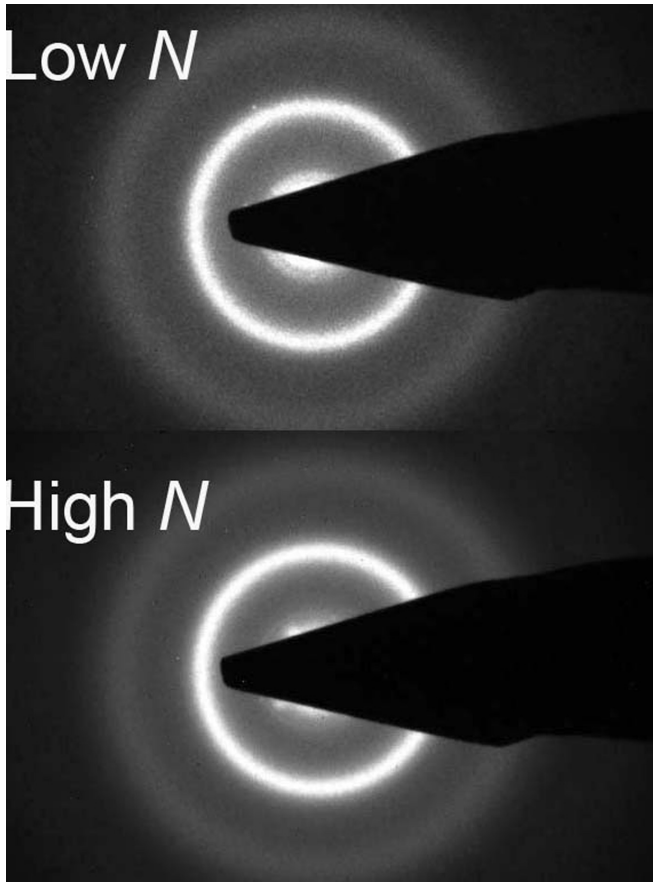


FIG. 7. Electron diffraction patterns for two In_xO films deposited on carbon-coated Cu grids. Both films have identical thicknesses of $d \approx 20$ nm (determined by the quartz-crystal monitor). The top pattern, labeled low- N , has $N \approx 1 \times 10^{19} \text{ cm}^{-3}$ while the high- N sample has $N \approx 9 \times 10^{20} \text{ cm}^{-3}$. The patterns appear quite similar but a careful comparison of intensity shows an overall higher signal in the indium-rich film. This is due to that the dominant signal is determined by the indium atoms.

position of the boson peak [23]. Therefore, migration of oxygen is plausibly the underlying mechanism for the changes in the spatial rearrangement of oxygen vacancies that take place during heat treatment.

To be consistent with our observations, the oxygen diffusion coefficient D_{O} should be no smaller than $\approx 10^{-12} \text{ cm}^2/\text{s}$; this will make it feasible for oxygen to diffuse over a region $L \approx 5 \mu\text{m}$ during a time $\tau \approx 2$ days, the duration of heat treatment in the present study. This value is comparable with conventionally measured D_{O} for oxygen diffusion in several solids [48] and in a polymer glass [49] (extrapolating results of these studies to the typical temperature used in the heat treatment, $T \approx 360$ K). Actually, the presence of vacancies probably makes oxygen diffusion in these In_xO thin films faster than in the bulk solids we compare it with.

The dynamics of processes that occur on a microscopic scales depends on multistage bond formation and local structure rearrangement [24,50] that probably involves many-particle coordinated transitions.

In addition to the sample conductance, a feature that is affected by these short-range processes is the film surface

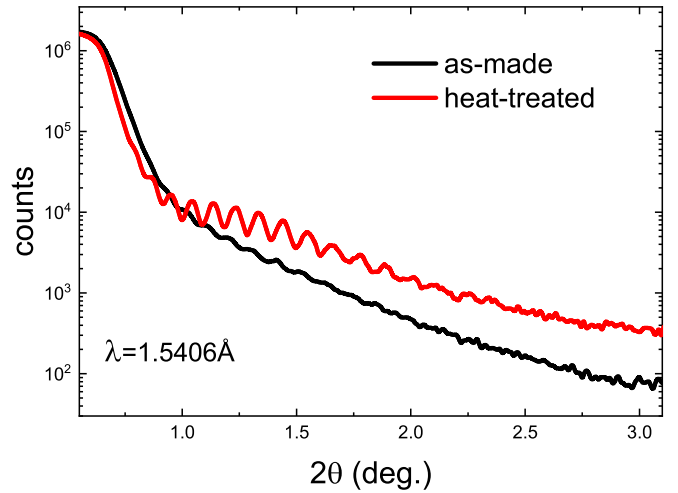


FIG. 8. X-ray reflectometry spectra for a high- N sample ($N \approx 8.5 \times 10^{20} \text{ cm}^{-3}$) version of In_xO film having similar composition as that of the sample in Fig. 1 but with a thickness $d = 71$ nm. Plots are shown for the before-and-after heat treatment at 360 ± 5 K for 14 hours. This resulted in the sheet resistance of the film to decrease from $R_{\square} = 6.8 \text{ k}\Omega$ to $R_{\square} = 3.12 \text{ k}\Omega$. Curves are displaced along the ordinate for clarity.

roughness. This aspect may be probed by x-ray interferometry (XRR) using typically a subnanometer wavelength radiation. An example of XRR spectra taken before and after a brief heat treatment of a high- N In_xO film is shown in Fig. 8.

The enhanced visibility of the XRR interference pattern following heat treatment is the result of a more homogeneous distribution of defects. These processes take place on a microscopic scale, directly affecting the conductivity via changes in the basic transport parameters such as mean-free-path, or the hopping length in the diffusive or hopping regime respectively.

The effect on conductivity due to homogenization of the *mesoscopic* regions probed by the Raman scattering is a more intricate issue. The length scale relevant for conductivity in In_xO films are much smaller than a few microns whether the system is on the metallic or insulating side of the transition even at cryogenic temperatures.

As mentioned above, the macroscopic carrier concentration of the sample is essentially unchanged during heat treatment. Local changes in N , on the other hand, do occur as evidenced by the Raman data (Figs. 1 and 2). These changes may increase the conductance of a given region while decreasing the conductance of another region (to be consistent with the global condition on N). The change in the macroscopic conductance due to these homogenization events will therefore be small except deep in the insulating side where the sample conductance would increase due to the logarithmic averaging inherent to the hopping regime [51,52].

In summary, we examined in this paper the relation between disorder and spatial uniformity of the potential perceived by the charge carriers in an amorphous metal. Films of In_xO with different carrier concentration but similar $k_{\text{F}}\ell$ were used to represent systems that differ significantly by their absolute degree of disorder. Both systems exhibit the same “frozen-liquid” structure with essentially indistinguishable

diffraction patterns but they differ in their “defects” density determined by their chemical composition. It is shown that the film with the stronger disorder exhibits a higher degree of heterogeneity extending over mesoscopic scales. Moreover, reducing the disorder in the film by heat treating it, resulted in a decrease in heterogeneity over both microscopic, and mesoscopic scales. In this case the change of disorder that resulted from the treatment is characterized by the Ioffe-Regel parameter acting as a relative measure of disorder. Disorder in In_xO is presumably dominated by the local concentration of oxygen vacancies that play the dual role as dopants and scatterers. Charge carriers that originate from off-stoichiometry conditions is a common scenario in many oxygen-deficient metal-oxides including high- T_C compounds. It would be interesting to see how general is the relation between disorder and heterogeneity in these compounds and in other disordered materials.

Another corollary implicit to the arguments raised above is that local defects, the oxygen vacancies in the current system, contribute to ρ_{RT} more than the lack of long-range order associated with amorphicity. This means that, for the same $k_F\ell$, the larger is the In/O ratio, the larger is the contribution of the diagonal component to the system disorder. This makes In_xO a useful platform to study experimentally the relative role of the two types of disorder.

ACKNOWLEDGMENTS

The assistance by Dr. Anna Radko with the Raman spectra work is gratefully acknowledged. This research has been partially supported by the Grant No. 1030/16 administered by the Israel Academy for Sciences and Humanities.

-
- [1] B. Derrida, Can disorder induce several phase transitions? *Phys. Rep.* **103**, 29 (1984).
- [2] M. Inui, S. A. Trugman, and E. Abrahams, Unusual properties of midband states in systems with off-diagonal disorder, *Phys. Rev. B* **49**, 3190 (1994).
- [3] M. A. Ramos, S. Vieira, F. J. Bermejo and J. Dawidowski, H. E. Fischer, H. Schober, M. A. González, C. K. Loong and D. L. Price, Quantitative Assessment of the Effects of Orientational and Positional Disorder on Glassy Dynamics, *Phys. Rev. Lett.* **78**, 82 (1997).
- [4] T. Bellini, M. Buscaglia, C. Chiccoli, F. Mantegazza, P. Pasini, and C. Zannoni, Nematics with Quenched Disorder: What Is Left when Long Range Order Is Disrupted? *Phys. Rev. Lett.* **85**, 1008 (2000).
- [5] S. Balibar and F. Caupin, Supersolidity and disorder, *J. Phys.: Condens. Matter* **20**, 173201 (2008).
- [6] P. Titum, N. H. Lindner, M. C. Rechtsman, and G. Refael, Disorder-Induced Floquet Topological Insulators, *Phys. Rev. Lett.* **114**, 056801 (2015).
- [7] S. Grozdanov, A. Lucas, S. Sachdev, and K. Schalm, Absence of Disorder-Driven Metal-Insulator Transitions in Simple Holographic Models, *Phys. Rev. Lett.* **115**, 221601 (2015).
- [8] F. Baboux, L. Ge, T. Jacqmin, M. Biondi, E. Galopin, A. Lemaître, L. Le Gratiet, I. Sagnes, S. Schmidt, H. E. Türeci, A. Amo, and J. Bloch, Bosonic Condensation and Disorder-Induced Localization in a Flat Band, *Phys. Rev. Lett.* **116**, 066402 (2016).
- [9] T. Vojta, Disorder in Quantum Many-Body Systems, *Annu. Rev. Condens. Matter Phys.* **10**, 233 (2019).
- [10] M. E. Raikh and E. V. Tsiper, Energy spectrum and size quantization in partially ordered semiconductor alloys, *Phys. Rev. B* **49**, 2509 (1994).
- [11] V. M. Apalkov and M. E. Raikh, Universal fluctuations of the random lasing threshold in a sample of a finite area, *Phys. Rev. B* **71**, 054203 (2005); T. A. Sedraky, E. G. Mishchenko, and M. E. Raikh, Zero-Bias Tunneling Anomaly in a Clean 2D Electron Gas Caused by Smooth Density Variations, *Phys. Rev. Lett.* **99**, 206405 (2007).
- [12] Z. Ovadyahu, Some finite temperature aspects of the Anderson transition, *J. Phys. C: Solid State Phys.* **19**, 5187 (1986).
- [13] D. B. Buchholz, Q. Ma, D. Alducin, A. Ponce, M. Jose-Yacamán, R. Khanal, J. E. Medvedeva, and R. P. H. Chang, The structure and properties of amorphous indium oxide, *Chem. Mater.* **26**, 5401 (2014).
- [14] D. Shahar and Z. Ovadyahu, Superconductivity near the mobility edge, *Phys. Rev. B* **46**, 10917 (1992).
- [15] V. Gantmakher, Transport properties of normal and quasinormal states of poor superconductors, *Int. J. Mod. Phys. B* **12**, 3151 (1998).
- [16] D. Kowal and Z. Ovadyahu, Disorder induced granularity in an amorphous superconductor, *Solid State Commun.* **90**, 783 (1994).
- [17] G. Sambandamurthy, L. W. Engel, A. Johansson, and D. Shahar, Superconductivity-Related Insulating Behavior, *Phys. Rev. Lett.* **92**, 107005 (2004).
- [18] S. Poran, E. Shimshoni, and A. Frydman, Disorder-induced superconducting ratchet effect in nanowires, *Phys. Rev. B* **84**, 014529 (2011).
- [19] B. Sacépé, T. Dubouchet, C. Chapelier, M. Sanquer, M. Ovadia, D. Shahar, M. Feigel'man, and L. Ioffe, Localization of preformed Cooper pairs in disordered superconductors, *Nat. Phys.* **7**, 239 (2011).
- [20] D. Sherman, G. Kopnov, D. Shahar, and A. Frydman, Measurement of a Superconducting Energy Gap in a Homogeneously Amorphous Insulator, *Phys. Rev. Lett.* **108**, 177006 (2012).
- [21] Y. Lee, A. Frydman, T. Chen, B. Skinner, and A. M. Goldman, Electrostatic tuning of the properties of disordered indium-oxide films near the superconductor-insulator transition, *Phys. Rev. B* **88**, 024509 (2013).
- [22] D. Sherman, U. S. Pracht, B. Gorshunov, S. Poran, J. Jesudasan, M. Chand, P. Raychaudhuri, M. Swanson, N. Trivedi, A. Auerbach *et al.*, The Higgs mode in disordered superconductors close to a quantum phase transition, *Nat. Phys.* **11**, 188 (2015).
- [23] I. Zbeda, I. Bar, and Z. Ovadyahu, Microstructure and the boson peak in thermally treated In_xO films, *Phys. Rev. Mater.* **5**, 085602 (2021).

- [24] Z. Ovadyahu, Memory versus irreversibility in the thermal densification of amorphous glasses, *Phys. Rev. B* **95**, 214207 (2017); Structure dynamics in thermal-treatment of amorphous indium-oxide films, *Phys. Status Solidi B* **257**, 1900310 (2020).
- [25] U. Givan and Z. Ovadyahu, Compositional disorder and transport peculiarities in the amorphous indium-oxides, *Phys. Rev. B* **86**, 165101 (2012).
- [26] S. R. Elliott, A unified model for the low-energy vibrational behavior of amorphous solids, *Europhys. Lett.* **19**, 201 (1992)
- [27] W. Schirmacher, G. Diezemann, and C. Ganter, Harmonic Vibrational Excitations in Disordered Solids and the “Boson Peak”, *Phys. Rev. Lett.* **81**, 136 (1998).
- [28] H. Shintani and H. Tanaka, Universal link between the boson peak and transverse phonons in glass, *Nat. Mater.* **7**, 870 (2008).
- [29] V. L. Gurevich, D. A. Parshin, and H. R. Schober, Pressure dependence of the boson peak in glasses, *Phys. Rev. B* **71**, 014209 (2005).
- [30] H. R. Schober, U. Buchenau, and V. L. Gurevich, Pressure dependence of the boson peak in glasses: Correlated and uncorrelated perturbations, *Phys. Rev. B* **89**, 014204 (2014).
- [31] V. K. Malinovsky and A. P. Sokolov, The nature of boson peak in Raman scattering in glasses, *Solid State Commun.* **57**, 757 (1986).
- [32] W. Schirmacher, T. Scopigno, and G. Ruocco, Theory of vibrational anomalies in glasses, *J. Non-Cryst. Solids* **407**, 133 (2015).
- [33] Z. Ovadyahu, B. Ovrin and H. W. Kraner, Microstructure and electro-optical properties of evaporated indium-oxide Films, *J. Electrochem. Soc.* **130**, 917 (1983).
- [34] A. Zawadowski and M. Cardona, Theory of Raman scattering on normal metals with impurities, *Phys. Rev. B* **42**, 10732 (1990).
- [35] R. Nemetschek, M. Opel, C. Hoffmann, P. F. Müller, R. Hackl, H. Berger and L. Forró, A. Erb and E. Walker, Pseudogap and Superconducting Gap in the Electronic Raman Spectra of Underdoped Cuprates, *Phys. Rev. Lett.* **78**, 4837 (1997).
- [36] J. A. Hoyos, C. Kotabage, and T. Vojta, Effects of Dissipation on a Quantum Critical Point with Disorder, *Phys. Rev. Lett.* **99**, 230601 (2007).
- [37] S. Ubaid-Kassis, T. Vojta, and A. Schroeder, Quantum Griffiths phase in the weak itinerant ferromagnetic alloy $\text{Ni}_{1-x}\text{V}_x$, *Phys. Rev. Lett.* **104**, 066402 (2010).
- [38] R. Wang, A. Gebretsadik, S. Ubaid-Kassis, A. Schroeder, T. Vojta, P. J. Baker, F. L. Pratt, S. J. Blundell, T. Lancaster, I. Franke, J. S. Möller, and K. Page, Quantum Griffiths Phase Inside the Ferromagnetic Phase of $\text{Ni}_{1-x}\text{V}_x$, *Phys. Rev. Lett.* **118**, 267202 (2017).
- [39] Y. Xing, K. Zhao, P. Shan, F. Zheng, Y. Zhang, H. Fu, Y. Liu, M. Tian, C. Xi, H. Liu, J. Feng, X. Lin, S. Ji, X. Chen, Q.-K. Xue, and J. Wang, Ising superconductivity and quantum phase transition in macro size monolayer NbSe_2 , *Nano Lett.* **17**, 6802 (2017).
- [40] Y. Saito, T. Nojima, and Y. Iwasa, Quantum phase transitions in highly crystalline two-dimensional superconductors, *Nat. Commun.* **9**, 778 (2018).
- [41] N. A. Lewellyn, I. M. Percher, J. Nelson, J. Garcia-Barriocanal, I. Volotsenko, A. Frydman, T. Vojta, and A. M. Goldman, Infinite-randomness fixed point of the quantum superconductor-metal transitions in amorphous thin films, *Phys. Rev. B* **99**, 054515 (2019); P. Reiss, D. Graf, A. A. Haghighirad, T. Vojta, and A. I. Coldea, Signatures of a Quantum Griffiths Phase Close to an Electronic Nematic Quantum Phase Transition, *Phys. Rev. Lett.* **127**, 246402 (2021).
- [42] Z. Ovadyahu, Slow dynamics of the electron-glasses: The role of disorder, *Phys. Rev. B* **95**, 134203 (2017).
- [43] E. Yamaguchi, H. Aoki and H. Kamimura, Intra- and interstate interactions in Anderson localised states, *J. Phys. C: Solid State Phys.* **12**, 4801 (1979); H. Kamimura, Theoretical model on the interplay of disorder and electron correlations, *Prog. Theor. Phys. Suppl.* **72**, 206 (1982).
- [44] Z. Ovadyahu, Interaction-induced spatial correlations in a disordered glass, *Phys. Rev. B* **105**, 235101 (2022).
- [45] The samples in figure 6 are part of a fuller study described in [42].
- [46] O. Cohen and Z. Ovadyahu, Resistance noise near the Anderson transition, *Phys. Rev. B* **50**, 10442 (1994).
- [47] F. N. Hooge, $1/f$ noise is no surface effect, *Phys. Lett. A* **29**, 139 (1969).
- [48] R. Kirchheim, Metals as sinks and barriers for interstitial diffusion with examples for oxygen diffusion in copper, niobium, and tantalum, *Acta Metall.* **27**, 869 (1979).
- [49] L. Poulsen and P. R. Ogilby, Oxygen diffusion in glassy polymer films: Effects of other gases and changes in pressure, *J. Phys. Chem. A* **104**, 2573 (2000).
- [50] Yu. M. Galperin, V. L. Gurevich, and D. A. Parshin, Theory of low-temperature thermal expansion of glasses, *Phys. Rev. B* **32**, 6873 (1985).
- [51] H. L. Zhao, B. Z. Spivak, M. P. Gelfand, and S. Feng, Negative magnetoresistance in variable-range-hopping conduction, *Phys. Rev. B* **44**, 10760 (1991).
- [52] O. Entin-Wohlman, Y. Imry, and U. Sivan, Orbital magnetoconductance in the variable-range-hopping regime, *Phys. Rev. B* **40**, 8342 (1989).